SIAM J. APPL. MATH.
Vol. 78, No. 2, pp. 1078–1104

ZOOLOGY OF A NONLOCAL CROSS-DIFFUSION MODEL FOR TWO SPECIES*

JOSÉ A. CARRILLO†, YANGHONG HUANG‡, AND MARKUS SCHMIDTCHEN†

Abstract. We study a nonlocal two species cross-interaction model with cross-diffusion. We propose a positivity preserving finite volume scheme based on the numerical method introduced in [J. A. Carrillo, A. Chertock, and Y. Huang, *Commun. Comput. Phys.*, 17 (2015), pp. 233–258] and explore this new model numerically in terms of its long-time behaviors. Using the so-gained insights, we compute analytical stationary states and travelling pulse solutions for a particular model in the case of attractive-attractive/attractive-repulsive cross-interactions. We show that, as the strength of the cross-diffusivity decreases, there is a transition from adjacent solutions to completely segregated densities, and we compute the threshold analytically for attractive-repulsive cross-interactions. Other bifurcating stationary states with various coexistence components of the support are analyzed in the attractive-attractive case. We find a strong agreement between the numerically and the analytically computed steady states in these particular cases, whose main qualitative features are also present for more general potentials.

Key words. cross-diffusion, nonlocal aggregation-diffusion systems, volume exclusion

AMS subject classifications. 35K55, 65N08, 35C05

DOI. 10.1137/17M1128782

1. Introduction.

Multiagent systems in nature oftentimes exhibit emergent behavior, i.e., the formation of patterns in the absence of a leader or external stimuli such as light or food sources. The most prominent examples of these phenomena are probably fish schools, flocking birds, and herding sheep, reaching across scales from tiny bacteria to huge mammals.

While self-interaction models for one particular species have been extensively studied (cf. [26, 23, 20, 38, 47] and references therein), there has been a growing interest in understanding and modelling interspecific interactions, i.e., the interaction among different types of species. One way to derive macroscopic models from microscopic dynamics consists of taking suitable scaling limits as the number of individuals goes to infinity. Minimal models for collective behavior include attraction and/or repulsion between individuals as the main source of interaction; see [47, 19, 20, 35] and the references therein. Attraction and repulsion are normally introduced through effective pairwise potentials whose strength and scaling properties determine the limiting continuum equations; see [40, 9, 8, 16]. Usually, localized strong repulsion gives rise to nonlinear diffusion like that in porous medium type models [40], while long-range attraction remains nonlocal in the final macroscopic equation; see [16] and the references therein.

In this paper we propose a finite volume scheme to study two-species systems of

*Received by the editors May 4, 2017; accepted for publication (in revised form) January 25, 2018; published electronically April 5, 2018.
http://www.siam.org/journals/siap/78-2/M112878.html
Funding: The first author's work was partially supported by the Royal Society via a Wolfson Research Merit Award and by EPSRC grant EP/P031587/1.

†Department of Mathematics, Imperial College London, SW7 2AZ London, UK (carrillo@imperial.ac.uk, m.schmidtchen15@imperial.ac.uk).
‡School of Mathematics, The University of Manchester, Manchester M13 9PL, UK (yanghong.huang@manchester.ac.uk).

the form

$$\partial_t \rho = \nabla \cdot \Big(\rho \nabla \big(W_{11} \star \rho + W_{12} \star \eta + \epsilon(\rho + \eta) \big) \Big), \tag{1a}$$

$$\partial_t \eta = \nabla \cdot \Big(\eta \nabla \big(W_{22} \star \eta + W_{21} \star \rho + \epsilon(\rho + \eta) \big) \Big), \tag{1b}$$

with given initial data

$$\rho(x,0) = \rho_0(x) \qquad \text{and} \qquad \eta(x,0) = \eta_0(x). \tag{1c}$$

Here, ρ, η are two unknown mass densities, W_{11}, W_{22} are self-interaction potentials (or intraspecific interaction potentials), W_{12}, W_{21} are cross-interaction potentials (or interspecific interaction), and $\epsilon > 0$ is the coefficient of the cross-diffusivity. The nonlinear diffusion term of porous medium type can be considered as a mechanism to include volume exclusion in cell chemotaxis [32, 41, 12], since it corresponds to very concentrated repulsion between all individuals.

This model can also be easily understood as a natural extension of the well-known aggregation equation (cf. [38, 47, 3, 18]) to two species including a cross-diffusion term. Common interaction potentials for the one species case include power laws $W(x) = |x|^p/p$, as, for instance, in the case of granular media models; cf. [2, 48]. Another choice is a combination of power laws of the form $W(x) = |x|^a/a - |x|^b/b$, for $-d < b < a$ where d is the space dimension. These potentials, featuring short-range repulsion and long-range attraction, are typically chosen in the context of swarming models; cf. [36, 1, 28, 29, 4, 21, 17]. Other typical choices include characteristic functions of sets (like spheres) or Morse potentials

$$W(x) = -c_a \exp(-|x|/l_a) + c_r \exp(-|x|/l_r),$$

or their regularized versions $W_p(x) = -c_a \exp(-|x|^p/l_a) + c_r \exp(-|x|^p/l_r)$, where c_a, c_r and l_a, l_r denote the interaction strength and radius of the attractive (resp., repulsive) part and $p \geq 2$; cf. [26, 22, 21]. These potentials display a decaying interaction strength, e.g., accounting for biological limitations of visual, acoustic, or olfactory sense. The asymptotic behavior of solutions to one single equation where the repulsion is modelled by nonlinear diffusion and the attraction by nonlocal forces has also received lots of attention in terms of qualitative properties, stationary states, and metastability; see [11, 15, 27, 13, 14] and the references therein.

Systems without cross-diffusion, $\epsilon = 0$, were proposed in [24, 37] as the formal mean-field limit of the following ODE system:

$$\dot{x}_i = -\frac{1}{N} \sum_{j \neq i} \nabla W_{11}(x_i - x_j) - \frac{1}{M} \sum_{j \neq i} \nabla W_{12}(x_i - y_j),$$

$$\dot{y}_i = -\frac{1}{M} \sum_{j \neq i} \nabla W_{22}(y_i - y_j) - \frac{1}{N} \sum_{j \neq i} \nabla W_{21}(y_i - x_j).$$

Various explicit solutions of codimension one, together with their stability, were studied in [37]. If this system is symmetrizable in the sense that $W_{12} = \alpha W_{21}$ for some positive constant $\alpha > 0$, then it has an interaction energy functional nonincreasing along time. As a result, the system admits a gradient flow structure, and variational schemes can be applied to ensure existence of solutions; cf. [24, 33]. However, such a condition on the cross-interaction potentials is too exclusive in the sense that lots of applications exhibit a lack of symmetry in the interactions between different species.

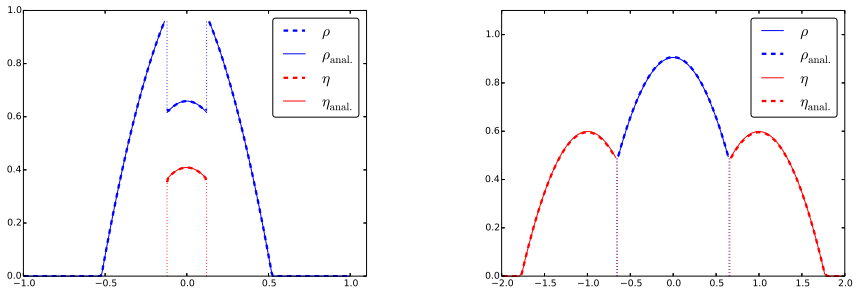

(a) Attractive-attractive cross interaction. (b) Attractive-repulsive cross interaction.

FIG. 1. *Steady states with jumps at the segregation or support boundaries. Left: Steady state showing coexistence for attractive-attractive cross interactions with jumps at the support boundaries of the surrounded species. Right: Steady state showing segregation for attractive-repulsive cross-interaction showing jumps at the segregation boundaries.*

In order to treat the system for general, and possibly different, cross-interactions W_{12} and W_{21}, the well-known variational scheme is modified in [24] to prove convergence even in the absence of gradient flow structure. These systems without cross-diffusion appear in modelling cell adhesion in mathematical biology with applications in zebrafish patterning and tumor growth models; see [30, 25, 42, 49] for instance.

In this paper we extend the cross-interaction model by a cross-diffusion term in [24], which is used to take into account the population pressure, i.e., the tendency of individuals to avoid areas of high population density. As cross-diffusion, we choose the form introduced by Gurtin and Pipkin in their seminal paper [31]. Although their work is antedated by results of mathematicians and biologists interested in density segregation effects of biological evolution equations (cf. [45, 44] and references therein), the particularity about their population pressure model is the occurrence of strict segregation of densities under certain circumstances; cf. [31, 6, 7]. This cross-diffusion term has been the basis to incorporate volume exclusions in models for tumor growth [5] or cell adhesion [39].

Hence, our model is of particular interest from a modelling point of view taking into account nonlocal interactions between the same species and different species as well as the urge of both species to avoid clustering. We discover a rich asymptotic behavior including phenomena such as segregation of densities, regions of coexistence, travelling pulses—all of which are observed in biological contexts; cf. [43, 46]. Existence of segregated stationary states under certain assumptions on the interaction potentials for small cross-diffusivity has been obtained recently in [10]. Here we show that it is in fact possible to find explicit stationary states and travelling pulses for certain singular yet not necessarily decaying interaction potentials showing coexistence and segregation of densities.

The stationary states and travelling pulses found in this work are relevant for several reasons. On the one hand, they showcase the main mathematical difficulties from the analytical viewpoint, since discontinuities in the densities appear at segregation points between species or at the boundaries of their supports, as shown in Figure 1. This phenomenon never occurs in aggregation-diffusion equations for a single species; see [47], for instance. Instead, basic a priori estimates show that the total population $\rho + \eta$ must be continuous for all times. However, any well-posedness results including

these steady profiles for the system (1) would need a control on the evolution in time of the BV-norms of both species separately which is not available.

On the other hand, these profiles, even if found for particular choices of the interaction potentials, allow for fine tuning of numerical schemes since they serve as validation tests for the numerical schemes to check if they respect the sharp boundaries. Our proposed numerical scheme does perform extremely well for this purpose as shown in Figure 1. Moreover, these features of the steady states and the travelling pulses are generic for a large family of potentials as shown below. Therefore, the main theoretical and numerical difficulties in these particular cases are shared by the whole family of system of PDEs in (1).

The rest of this paper is organized as follows: in section 2 we discuss the basic properties of the system (1) in one dimension, and in section 3 we propose our numerical scheme which is used in section 4 to explore the model and its long-time behavior numerically. These insights are used to make reasonable assumptions on the support of the asymptotic solutions in order to derive analytic expressions for their shape and give a first classification of the zoology of different stationary states. Finally, we discuss in section 5 how generic these phenomena are for different potentials, and we draw the final conclusions of this work in section 6.

2. A nonlocal cross-diffusion model for two species. Throughout this paper we consider system (1) in one spatial dimension. Then the model reads

$$\partial_t \rho = \partial_x(\rho \partial_x(W_{11} \star \rho + W_{12} \star \eta + \epsilon(\rho + \eta))), \tag{2a}$$

$$\partial_t \eta = \partial_x(\eta \partial_x(W_{22} \star \eta + W_{21} \star \rho + \epsilon(\rho + \eta))), \tag{2b}$$

for some initial data $\rho(x,0) = \rho_0(x)$, and $\eta(x,0) = \eta_0(x)$, and radially symmetric potentials W_{ij}, for $i,j = 1,2$. Furthermore let m_1 and m_2 denote the mass of ρ and of η, respectively. We can obtain some a priori estimates on solutions by using the following energy:

$$\mathcal{E}(\rho,\eta) = \int_{\mathbb{R}} \rho \log \rho \, \mathrm{d}x + \int_{\mathbb{R}} \eta \log \eta \, \mathrm{d}x.$$

We note that for $W_{ij} \in W^{2,\infty}(\mathbb{R})$, along any solution (ρ,η) of system (2), there formally holds

$$\begin{aligned}
\frac{\mathrm{d}}{\mathrm{d}t}\mathcal{E}(\rho,\eta) = & -\int \epsilon[\partial_x(\rho+\eta)]^2 \mathrm{d}x \\
& - \int \partial_x\rho\, \partial_x\big(W_{11} \star \rho + W_{12} \star \eta\big)\mathrm{d}x - \int \partial_x\eta\, \partial_x\big(W_{22} \star \eta + W_{21} \star \rho\big)\mathrm{d}x \\
\leq & -\int \epsilon|\partial_x(\rho+\eta)|^2 \mathrm{d}x \\
& + \int \rho\partial_x^2\big(W_{11} \star \rho + W_{12} \star \eta\big)\mathrm{d}x + \int \eta\partial_x^2\big(W_{22} \star \eta + W_{21} \star \rho\big)\mathrm{d}x,
\end{aligned}$$

that is

$$\frac{\mathrm{d}}{\mathrm{d}t}\mathcal{E}(\rho,\eta) \leq C - \int_{\mathbb{R}} \epsilon|\partial_x(\rho+\eta)|^2 \mathrm{d}x.$$

In the case of $W_{ii} = C_{ii}x^2/2$ and $W_{ij} = \pm C_{ij}|x|$ for $i \neq j$ with nonnegative constants C_{ij}, the above estimate is also true, since

$$\int \rho\partial_x^2 W_{11} \star \rho \mathrm{d}x = C_{11}m_1 \int \rho \mathrm{d}x = C_{11}m_1^2, \quad \left| \int \rho\partial_x^2 W_{ij} \star \eta \mathrm{d}x \right| \leq 2C_{ij} \int \rho\eta < \infty,$$

and similarly for the terms in (2b), as long as $\rho, \eta \in L^\infty(0,T;L^\infty(\mathbb{R}))$. Thus the terms $\int \rho\partial_x^2(W_{11}\star\rho + W_{12}\star\eta)\mathrm{d}x$ and similarly $\int \eta\partial_x^2(W_{22}\star\eta + W_{21}\star\rho)\mathrm{d}x$ are bounded. Therefore, we conclude that

$$\frac{\mathrm{d}}{\mathrm{d}t}\mathcal{E}(\rho,\eta) \le C - \int_{\mathbb{R}} \epsilon|\partial_x(\rho+\eta)|^2\mathrm{d}x,$$

implying that $\rho+\eta \in L^2(0,T;H^1(\mathbb{R}))$. We deduce that the sum of both species remains continuous for almost all positive times—a property we will make use of later. Now, let us introduce our notion of steady states.

DEFINITION 2.1 (steady states). *A pair of functions (ρ,η) defined on $\mathbb{R}$ is called a steady state to* (2) *if both functions are integrable and bounded, $\rho,\eta \in L^1(\mathbb{R})\cap L^\infty(\mathbb{R})$, such that their sum satisfies $\sigma := \rho+\eta \in H^1(\mathbb{R})$ and there holds*

$$0 = \partial_x(\rho\partial_x(W_{11}\star\rho + W_{12}\star\eta + \epsilon(\rho+\eta))),$$
$$0 = \partial_x(\eta\partial_x(W_{22}\star\eta + W_{21}\star\rho + \epsilon(\rho+\eta)))$$

in the distributional sense.

PROPOSITION 2.2 (almost characterization of steady states). *Any pair of functions $\rho,\eta \in L^1(\mathbb{R})\cap L^\infty(\mathbb{R})$ satisfying $\rho+\eta \in H^1(\mathbb{R})$ such that any connected component of their supports has nonempty interior is a steady state of system* (2) *if and only if there exist constants $c_1, c_2 \in \mathbb{R}$, possibly different on different connected components of the supports, such that*

$$\begin{aligned} c_1 &= W_{11}\star\rho + W_{12}\star\eta + \epsilon(\rho+\eta),\\ c_2 &= W_{22}\star\eta + W_{21}\star\rho + \epsilon(\rho+\eta). \end{aligned} \tag{3}$$

Proof. Clearly, the characterization is sufficient, since the velocity field vanishes in each connected component of their supports if there exist constants c_1, c_2 such that (3) are satisfied. Conversely, if there holds

$$0 = \partial_x(\rho\partial_x(W_{11}\star\rho + W_{12}\star\eta + \epsilon(\rho+\eta))),$$
$$0 = \partial_x(\eta\partial_x(W_{22}\star\eta + W_{21}\star\rho + \epsilon(\rho+\eta))),$$

we note that $\rho, \eta, \partial_x(\rho+\eta) \in L^2(\mathbb{R})$ by the definition of steady state, and therefore, the right-hand sides are distributional derivatives of L^1 functions. By a well-known result (cf., e.g., [34, Lemma 1.2.1]), we deduce that there exist constants $K_1, K_2 \in \mathbb{R}$ such that

$$K_1 = \rho\partial_x(W_{11}\star\rho + W_{12}\star\eta + \epsilon(\rho+\eta)),$$
$$K_2 = \eta\partial_x(W_{22}\star\eta + W_{21}\star\rho + \epsilon(\rho+\eta)).$$

Due to the integrabilty properties of the right-hand sides above, we infer that $K_1 = K_2 = 0$, and thus in the interior of any connected component of the supports of ρ and η, we obtain that there exist constants $c_1, c_2 \in \mathbb{R}$ such that

$$c_1 = W_{11}\star\rho + W_{12}\star\eta + \epsilon(\rho+\eta),$$
$$c_2 = W_{22}\star\eta + W_{21}\star\rho + \epsilon(\rho+\eta),$$

using the same argument as above. ∎

Note that the assumption on the interiors of the supports of the species is purely technical and is due to the regularity assumptions on our definition of stationary states. This avoids pathological cases such as functions supported on a fat Cantor set.

3. Numerical scheme. In order to solve system (2), we introduce a finite volume scheme based on [15]. The problem is posed on the domain $\Omega := [-L, L]$ which is divided into N equal control volumes $(C_i)_{i=1,\dots,N}$, with $C_i := [x_{i-1/2}, x_{i+1/2}]$ and uniform size $\Delta x := x_{i+1/2} - x_{i-1/2}$. Finally, the time interval $[0, T]$ is discretized by $t^n = n\Delta t$, for $n = 0, \dots, \lceil T/\Delta t \rceil$. We define the discretized initial data via

$$\rho_i^0 := \frac{1}{\Delta x}\int_{C_i} \rho_0(x)\mathrm{d}x \qquad \text{and} \qquad \eta_i^0 := \frac{1}{\Delta x}\int_{C_i} \eta_0(x)\mathrm{d}x.$$

We integrate system (2) over the test cell $[t^n, t^{n+1}] \times C_i$ to obtain

$$\begin{aligned} \int_{C_i} \rho(t^{n+1}, x)\mathrm{d}x &= \int_{C_i} \rho(t^n, x)\mathrm{d}x - \Delta t\big(\bar{F}^n_{i+1/2} - \bar{F}^n_{i-1/2}\big), \\ \int_{C_i} \eta(t^{n+1}, x)\mathrm{d}x &= \int_{C_i} \eta(t^n, x)\mathrm{d}x - \Delta t\big(\bar{G}^n_{i+1/2} - \bar{G}^n_{i-1/2}\big), \end{aligned} \tag{4}$$

where $\bar{F}^n_{i+1/2}, \bar{G}^n_{i+1/2}$ denote the flux on the boundary $x_{i+1/2}$ of cell C_i, i.e.,

$$\begin{aligned} \bar{F}^n_{i+1/2} &:= -\frac{1}{\Delta t}\int_{t^n}^{t^{n+1}} \big(\rho\partial_x(W_{11} \star \rho + W_{12} \star \eta + \epsilon(\rho + \eta))\big)(x_{i+1/2}, t)\mathrm{d}t, \\ \bar{G}^n_{i+1/2} &:= -\frac{1}{\Delta t}\int_{t^n}^{t^{n+1}} \big(\eta\partial_x(W_{22} \star \eta + W_{21} \star \rho + \epsilon(\rho + \eta))\big)(x_{i+1/2}, t)\mathrm{d}t. \end{aligned} \tag{5}$$

We define the cell averages

$$\rho_i^n := \frac{1}{\Delta x}\int_{C_i} \rho(t^n, x)\mathrm{d}x \quad \text{and} \quad \eta_i^n := \frac{1}{\Delta x}\int_{C_i} \eta(t^n, x)\mathrm{d}x,$$

and divide (4) by Δx to obtain the finite volume scheme

$$\begin{aligned} \rho_i^{n+1} &= \rho_i^n - \frac{\Delta t}{\Delta x}\left(F^n_{i+1/2} - F^n_{i-1/2}\right), \\ \eta_i^{n+1} &= \eta_i^n - \frac{\Delta t}{\Delta x}\left(G^n_{i+1/2} - G^n_{i-1/2}\right), \end{aligned} \tag{6a}$$

where we approximate the fluxes on the boundary, (5), by the numerical fluxes

$$\begin{aligned} F^n_{i+1/2} &= (U^n_{i+1/2})^+\rho_i^n + (U^n_{i+1/2})^-\rho^n_{i+1}, \\ G^n_{i+1/2} &= (V^n_{i+1/2})^+\eta_i^n + (V^n_{i+1/2})^-\eta^n_{i+1}, \end{aligned} \tag{6b}$$

using $(\cdot)^+ := \max(\cdot, 0)$ and $(\cdot)^- := \min(\cdot, 0)$ to denote the positive part and the negative part, respectively. The velocity is discretized by centered differences:

$$U^n_{i+1/2} = -\frac{\xi^n_{i+1} - \xi^n_i}{\Delta x} \qquad \text{and} \qquad V^n_{i+1/2} = -\frac{\zeta^n_{i+1} - \zeta^n_i}{\Delta x}. \tag{6c}$$

Here we have set

$$\begin{aligned} \xi_i^n &:= \Delta x \sum_k \left(W_{11}^{i-k}\rho_k^n + W_{12}^{i-k}\eta_k^n\right) + \epsilon(\rho_i^n + \eta_i^n), \\ \zeta_i^n &:= \Delta x \sum_k \left(W_{22}^{i-k}\eta_k^n + W_{21}^{i-k}\rho_k^n\right) + \epsilon(\rho_i^n + \eta_i^n), \end{aligned} \tag{6d}$$

where $W_{ij}^{l-k} = W_{ij}(x_l - x_k)$, for $i, j = 1, 2$. This scheme has proven to be very robust for one species, and under a (more restrictive) CFL condition we can also prove the following result.

PROPOSITION 3.1 (nonnegativity preservation). *Consider the system* (2) *with initial data* $\rho_0, \eta_0 \geq 0$. *Then for all* $n \in \mathbb{N}$ *the cell averages* ρ_i^n *and* η_i^n *obtained by the finite volume method* (6) *are also nonnegative, granted that the following CFL condition is satisfied:*

$$\Delta t \leq \frac{\Delta x}{2\max(\|U^n\|_\infty, \|V^n\|_\infty)}.$$

Proof. Let us assume that $\rho_i^n, \eta_i^n \geq 0$, and we need to show that then $\rho_i^{n+1}, \eta_i^{n+1} \geq 0$. According to (6a), (6b) we have

$$\begin{aligned}\rho_i^{n+1} &= \rho_i^n - \frac{\Delta t}{\Delta x}(F_{i+1/2}^n - F_{i-1/2}^n) \\ &= \rho_i^n - \frac{\Delta t}{\Delta x}\left[(U_{i+1/2}^n)^+\rho_i^n + (U_{i+1/2}^n)^-\rho_{i+1}^n - (U_{i-1/2}^n)^+\rho_{i-1}^n - (U_{i-1/2}^n)^-\rho_i^n\right].\end{aligned}$$

We can rearrange the terms so that

$$\begin{aligned}\rho_i^{n+1} = \rho_i^n &\left(1 - \frac{\Delta t}{\Delta x}\left[(U_{i+1/2}^n)^+ - (U_{i-1/2}^n)^-\right]\right) \\ &+ \frac{\Delta t}{\Delta x}(U_{i-1/2}^n)^+\rho_{i-1}^n - \frac{\Delta t}{\Delta x}(U_{i+1/2}^n)^-\rho_{i+1}^n.\end{aligned}$$

Clearly, all terms in the second line are nonnegative. The first line is nonnegative if the CFL condition is satisfied. Application of the same procedure to η_i^{n+1} yields the desired conclusion. ∎

4. Numerical study. In this section we study system (2) numerically with emphasis on its long-time behavior. Throughout this section we use the self-interaction potentials $W_{11}(x) := W_{22}(x) := x^2/2$ and the cross-interaction potentials $W_{12}(x) = W_{21}(x) = |x|$ or $W_{12}(x) = -W_{21}(x) = |x|$. These potentials are local approximations of the more popular Morse type potentials $W(x) = 1 - e^{-|x|^2/2}$ and $W(x) = 1 - e^{-|x|}$, such that many interesting steady patterns can still be reproduced in these simple settings. Moreover, this choice of potentials allows us to compute steady states of system (2) explicitly: $W_{11} * \rho$ and $W_{22} * \eta$ are essentially local, while W_{12} (and W_{21}) is proportional to the fundamental solution of the Laplacian (in one dimension here), commonly used in the literature for one species aggregation models; cf., e.g., [21, 11, 29]. We find a wide range of behaviors for the solutions, including segregation phenomena, for different cross-diffusivities and cross-interactions. Several assumptions have been made in the computation of explicit solutions below: from the translational invariance of the system (2), the centers of mass of both species are assumed to be constants; the supports of the solutions are taken to be intervals or union of intervals, motivated from numerical simulations and also expected from the nonlinear diffusion of porous medium type in the volume exclusion term.

This section is subdivided into two sections addressing the mutually attractive case and the attractive-repulsive case, respectively.

4.1. Attractive-attractive case. Let us begin with the case of attractive interaction between both species, i.e., $W_{12} = W_{21} = |x|$. Upon exploring the system numerically, we find a vast variety of stationary patterns, including both symmetric and nonsymmetric profiles whose occurrence and stability depend on the cross-diffusivity.

In fact, the coefficient ϵ of the cross-diffusivity plays a crucial role in the bifurcations of these profiles, and will be discussed in the next section. Then, we study the

system as the cross-diffusivity tends to zero and the stability of the steady states—a matter that seems closely intertwined with the bifurcations.

4.1.1. Steady states and behavioral bifurcation. We begin by introducing the two types of symmetric steady states observed in the attractive-attractive case. Motivated by numerical simulations, we assume that the stationary distributions are compactly supported, i.e.,

$$\operatorname{supp}(\rho) = [-c, c] \qquad \text{and} \qquad \operatorname{supp}(\eta) = [-b, b],$$

where $0 < b \le c$. The domain $[-c, -b] \cup [b, c]$ is then only inhabited by the first species but not η. Upon rearranging (3), we obtain

$$\rho(x) = -\frac{1}{\epsilon}\big(W_{11} \star \rho + W_{12} \star \eta - c_1\big), \tag{7}$$

for $x \in [-c, c]$. The two nonlocal terms $W_{11} \star \rho$ and $W_{12} \star \eta$ can be computed individually. First, the self-interaction terms become

$$W_{11} \star \rho(x) = \int W_{11}(x - y)\rho(y)\mathrm{d}y = \frac{1}{2}m_1 x^2 - M_1 x + \frac{1}{2}\bar{M}_1, \tag{8}$$

where

$$m_1 = \int_{\mathbb{R}} \rho(x)\mathrm{d}x, \quad M_1 = \int_{\mathbb{R}} x\rho(x)\mathrm{d}x, \quad \text{and} \quad \bar{M}_1 = \int_{\mathbb{R}} x^2\rho(x)\mathrm{d}x,$$

are the mass and the first two moments of ρ, respectively. Then the cross-interaction term becomes

$$W_{12} \star \eta(x) = \int |x - y|\eta(y)\mathrm{d}y = \begin{cases} M_2 - m_2 x, & x \in [-c, -b], \\ m_2 x - M_2, & x \in [b, c], \end{cases} \tag{9}$$

where m_2, M_2 denote the mass and the center of mass of the second species. Due to symmetry and translational invariance of the solution, both M_1 and M_2 can be taken as zero without loss of generality. Upon substitution of the nonlocal terms in (8) and (9), (7) is simplified into

$$\rho(x) = -\frac{1}{\epsilon}\left(\frac{1}{2}m_1 x^2 + \frac{1}{2}\bar{M}_1 \pm (-m_2 x) - c_1\right),$$

where "+" is for the case $x \in [-c, -b]$, and "−" for $x \in [b, c]$, respectively. Using the boundary condition $\rho(\pm c) = 0$ (in fact where $\rho + \eta$ vanishes identically), we get

$$\rho(x) = \begin{cases} -\dfrac{1}{2\epsilon}m_1(x^2 - c^2) + \dfrac{m_2}{\epsilon}(x + c), & x \in [-c, -b], \\ -\dfrac{1}{2\epsilon}m_1(x^2 - c^2) - \dfrac{m_2}{\epsilon}(x - c), & x \in [b, c]. \end{cases} \tag{10}$$

Finally, let us consider the interval $[-b, b]$ where both species coexist. Again, the first equation in (3) becomes

$$\begin{aligned} c_1 &= W_{11} \star \rho + W_{12} \star \eta + \epsilon(\rho + \eta) \\ &= \frac{1}{2}m_1 x^2 + \frac{1}{2}\bar{M}_1 + \epsilon(\rho + \eta) + \int_{-b}^{b} |x - y|\eta(y)\mathrm{d}y, \end{aligned} \tag{11}$$

where the cross-interaction term $W_{12} \star \eta$ can be further reduced, according to

$$\int_{-b}^{b} |x-y|\eta(y)\mathrm{d}y = x\int_{-b}^{x}\eta(y)\mathrm{d}y - \int_{-b}^{x} y\eta(y)\mathrm{d}y + \int_{x}^{b} y\eta(y)\mathrm{d}y - x\int_{x}^{b}\eta(y)\mathrm{d}y.$$

Notice that all terms on the right side are twice differentiable as a consequence of the fundamental theorem of calculus and the cancellations of some terms. Therefore, from (11), $\rho+\eta$ is twice differentiable in $(-b,b)$, and upon differentiating (11) twice we obtain

$$0 = (\rho+\eta)'' + \frac{2}{\epsilon}\eta + \frac{m_1}{\epsilon}, \tag{12}$$

and similarly from the second equation in (3)

$$0 = (\rho+\eta)'' + \frac{2}{\epsilon}\rho + \frac{m_2}{\epsilon}. \tag{13}$$

The system of equations (12) and (13) can be solved by first introducing the decoupled system for $u := \rho+\eta$ and $v := \rho-\eta$, given by

$$\begin{aligned} 2u'' + \frac{2}{\epsilon}u + \frac{m_1+m_2}{\epsilon} &= 0,\\ \frac{2}{\epsilon}v + \frac{m_2-m_1}{\epsilon} &= 0. \end{aligned}$$

Thus, the solutions ρ and η are obtained as

$$\rho(x) = \frac{\hat{u}_1}{2}\sin\left(\frac{x}{\sqrt{\epsilon}}\right) + \frac{\hat{u}_2}{2}\cos\left(\frac{x}{\sqrt{\epsilon}}\right) - \frac{m_2}{2}, \tag{14}$$

$$\eta(x) = \frac{\hat{u}_1}{2}\sin\left(\frac{x}{\sqrt{\epsilon}}\right) + \frac{\hat{u}_2}{2}\cos\left(\frac{x}{\sqrt{\epsilon}}\right) - \frac{m_1}{2}. \tag{15}$$

In fact, due to symmetry there holds $\hat{u}_1 = 0$, and (14), (15) can be simplified to

$$\rho(x) = \frac{\hat{u}_2}{2}\cos\left(\frac{x}{\sqrt{\epsilon}}\right) - \frac{m_2}{2}, \qquad \eta(x) = \frac{\hat{u}_2}{2}\cos\left(\frac{x}{\sqrt{\epsilon}}\right) - \frac{m_1}{2}. \tag{16}$$

Hence the symmetric steady states are determined uniquely by three parameters, $\hat{u}_2$, b, and c, which are governed by algebraic equations. Since η is only supported on $[-b,b]$, the condition for the total mass of η becomes

$$m_2 = \int_{-b}^{b}\eta(x)\mathrm{d}x = \sqrt{\epsilon}\hat{u}_2\sin\left(\frac{b}{\sqrt{\epsilon}}\right) - m_1 b,$$

which yields

$$\hat{u}_2 = \frac{m_2 + m_1 b}{\sqrt{\epsilon}\sin\left(\frac{b}{\sqrt{\epsilon}}\right)}.$$

From (10), (16), the condition for the total mass of ρ becomes

$$
\begin{aligned}
m_1 &= \left(\int_{-c}^{-b} + \int_{-b}^{b} + \int_{b}^{c}\right)\rho(x)\mathrm{d}x \\
&= \frac{m_1(b+2c)(c-b)^2}{3\epsilon} + \frac{m_2(c-b)^2}{\epsilon} + \sqrt{\epsilon}\hat{u}_2 \sin\left(\frac{b}{\sqrt{\epsilon}}\right) - m_2 b. \qquad (17)
\end{aligned}
$$

When $\hat{u}_2$ is eliminated, (17) provides a relation between b and c, i.e.,

$$
3\epsilon m_1 + 3\epsilon m_2 b = 3\epsilon(m_2 + m_1 b) + (c-b)^2(3m_2 + 2cm_1 + m_1 b). \qquad (18)
$$

Finally, consider the continuity of the sum of the densities $\rho+\eta$ at $x = b$ (cf. Definition 2.1),

$$
\lim_{x\uparrow b}\big(\rho(x)+\eta(x)\big) = \lim_{x\downarrow b}\big(\rho(x)+\eta(x)\big),
$$

whence

$$
m_1(c^2-b^2) + \epsilon m_1 + \epsilon m_2 + 2m_2(c-b) = 2\sqrt{\epsilon}(m_2 + m_1 b)\cot\left(\frac{b}{\sqrt{\epsilon}}\right). \qquad (19)
$$

Therefore, b and c are in the zero locus of (18), (19) that are numerically solved; cf. Figure 2(a). Then the shape of the steady state is given by two parabola profiles on the parts only inhabited by the first species and cosine profiles where both species coexist:

$$
\rho(x) = \begin{cases} -\dfrac{1}{2\epsilon}m_1(x^2-c^2) + \dfrac{m_2}{\epsilon}(x+c), & x \in [-c,-b], \\ \dfrac{\hat{u}_2}{2}\cos\left(\dfrac{x}{\sqrt{\epsilon}}\right) - \dfrac{m_2}{2}, & x \in [-b,b], \\ -\dfrac{1}{2\epsilon}m_1(x^2-c^2) - \dfrac{m_2}{\epsilon}(x-c), & x \in [b,c], \end{cases}
$$

and

$$
\eta(x) = \frac{\hat{u}_2}{2}\cos\left(\frac{x}{\sqrt{\epsilon}}\right) - \frac{m_1}{2},
$$

on $[-b,b]$. Figure 2(b) shows an excellent agreement between numerical and analytical Batman-like steady states. Let us remark that (18) implies $b = c$ in the case of $m_1 = m_2$. As a consequence both species completely overlap and the profile is just part of a cosine function as shown in Figure 3. Our simulations also suggest that the Batman profiles shown in Figure 2(b) gradually lose their stability as ϵ passes through two critical values $\epsilon^{(1)}$ and $\epsilon^{(2)}$ that can be determined numerically: for $\epsilon \in (0, \epsilon^{(1)}]$, the Batman profiles are the only symmetric stationary distribution; for $\epsilon \in (\epsilon^{(1)}, \epsilon^{(2)}]$, depending on the initial condition, a new family of symmetric profiles (called *the second kind*) emerges coexisting with the Batman profiles as in Figure 4; finally, for $\epsilon > \epsilon^{(2)}$ only profiles of the second kind prevail for given initial data. Since the steady states are a state of balance between diffusion and attractive interactions, the second kind of profiles can be seen as states in which the attractive force is not strong enough to ensure the formation of a single group for η as observed in the Batman profiles.

Similarly to the Batman profiles, we may determine parameters and their governing equations for profiles of the second kind. In the symmetric case, using (3) these

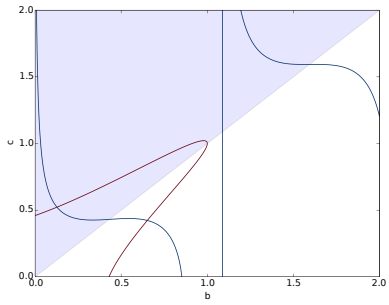

(a) The root of (18), (19) determines the support.

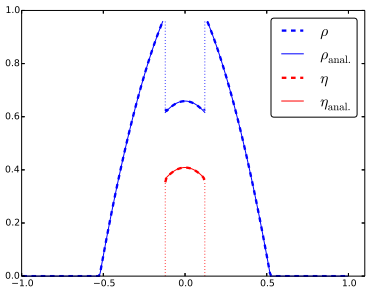

(b) $\epsilon = 0.12, m_1 = 0.6, m_2 = 0.1$.

FIG. 2. *Left: mass condition (red line) and the continuity of the sum (blue line) give rise to two equations for the support. The shaded area is the condition $c \geq b$. Right: analytical (straight lines) and numerical (dashed lines) Batman profiles agree perfectly. (Figure appears in color online.)*

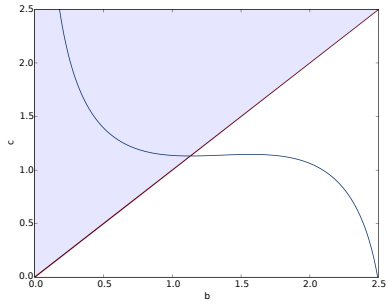

(a) The root of (18), (19) determines the support.

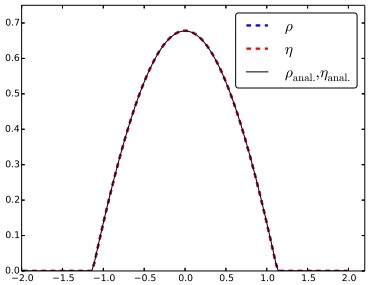

(b) $\epsilon = 1, m_1 = 1, m_2 = 1$.

FIG. 3. *Stationary distribution in the case of the same masses. Left: mass condition and continuity of the sum determine the support. Right: the analytical (straight lines) and the numerical (dashed lines) steady states agree perfectly.*

profiles can be determined in a similar way and are given by

$$\rho(x) = \begin{cases} \rho^L(x) & = \frac{1}{\epsilon}\left(\frac{m_2}{2}(d^2 - c^2) + m_1(d-c) + \frac{m_1}{2}(c^2 - x^2) + (1-p)m_2(c+x)\right), \\ \rho^M(x) & = \frac{B}{2}\cos\left(\frac{x}{\sqrt{\epsilon}}\right) - \frac{m_2}{2}, \\ \rho^R(x) & = \frac{1}{\epsilon}\left(\frac{m_2}{2}(d^2 - c^2) + m_1(d-c) + \frac{m_1}{2}(c^2 - x^2) + (1-p)m_2(c-x)\right), \end{cases}$$

where $\text{supp}(\rho^L) = [-c, -b], \text{supp}(\rho^M) = [-b, b]$, $\text{supp}(\rho^R) = [b, c]$, and p is the fraction of mass in the corners of η; cf. Figure 4 (areas filled in red). Similarly,

$$\eta(x) = \begin{cases} \eta^L(x) & = \frac{1}{\epsilon}\left(\frac{m_2}{2}(d^2 - x^2) + m_1(d+x)\right), \\ \eta^M(x) & = \frac{B}{2}\cos\left(\frac{x}{\sqrt{\epsilon}}\right) - \frac{m_1}{2}, \\ \eta^R(x) & = \frac{1}{\epsilon}\left(\frac{m_2}{2}(d^2 - x^2) + m_1(d-x)\right), \end{cases}$$

where $\text{supp}(\eta^L) = [-d, -c], \text{supp}(\eta^M) = [-b, b]$, and $\text{supp}(\eta^R) = [c, d]$. Obviously, there are five unknowns: b, c, d for the support, B for the amplitude in regions of

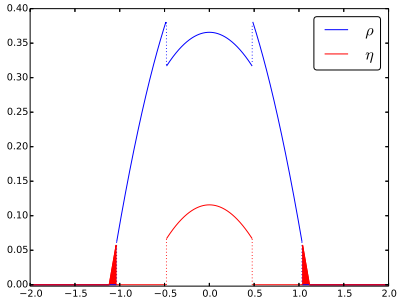

FIG. 4. *For $\epsilon > \epsilon^{(1)}$ a second kind of profile surfaces. In fact, there is a whole family of steady states parameterized by the mass fraction, $p \in [p_{\min}, p_{\max}]$, in the corners (filled in red).*

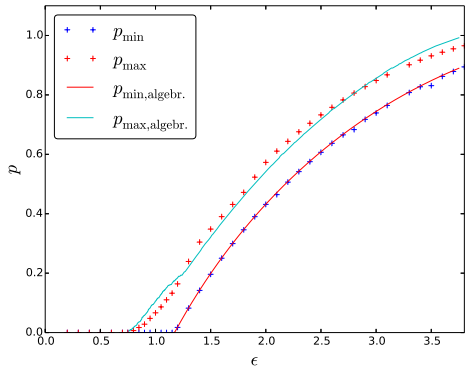

FIG. 5. *Depending on the cross-diffusivity we observe different symmetric steady states. The dashed curve shows the minimal mass fraction in the corner and the dotted line the maximal mass fraction leading to a stable stationary distribution.*

coexistence, and p for the mass fraction. Correspondingly, we find four conditions in order to determine all parameters but p:

$$pm_2 = 2\int_c^d \eta^R(x)\mathrm{d}x \qquad \text{and} \qquad (1-p)m_2 = \int_{-b}^{b} \eta^M(x)\mathrm{d}x,$$

for the mass near the corners and on the middle interval $[-b, b]$, respectively. Similarly, we know that

$$m_1 = \int_{-c}^{c} \rho(x)\mathrm{d}x, \qquad \text{and} \qquad \lim_{x\uparrow b}\sigma(x) = \lim_{x\downarrow b}\sigma(x), \qquad \text{and} \qquad \lim_{x\uparrow c}\sigma(x) = \lim_{x\downarrow c}\sigma(x),$$

for the mass of ρ and the continuity of the sum $\sigma = \rho + \eta$ at $x = c$ and $x = b$. Since p parameterizes a family of solutions and describes both branches (as envelopes) of the bifurcation diagram (cf. Figure 5), we are interested in finding the conditions leading to $p_{\min}(\epsilon), p_{\max}(\epsilon)$ in the diagram; see Figure 5. In order to determine the bifurcation diagram we run simulations with two different types of initial data—on the one hand we start the system with $\mathrm{supp}(\eta) \subset \mathrm{supp}(\rho)$, on the other hand we

initialize the system such that η is supported around ρ; cf. first row of Figure 6. The second row shows the stationary distribution asymptotically achieved with the respective initial data. We note that the mass fraction of η in the corners is different for both simulations albeit having used the same cross-diffusivity. The mass fraction in the left graph corresponds to $p = p_{\min}$ and the mass fraction in the right graph to $p = p_{\max}$, respectively. Now we want to give conditions determining the envelopes $p_{\min}(\epsilon), p_{\max}(\epsilon)$ of Figure 5.

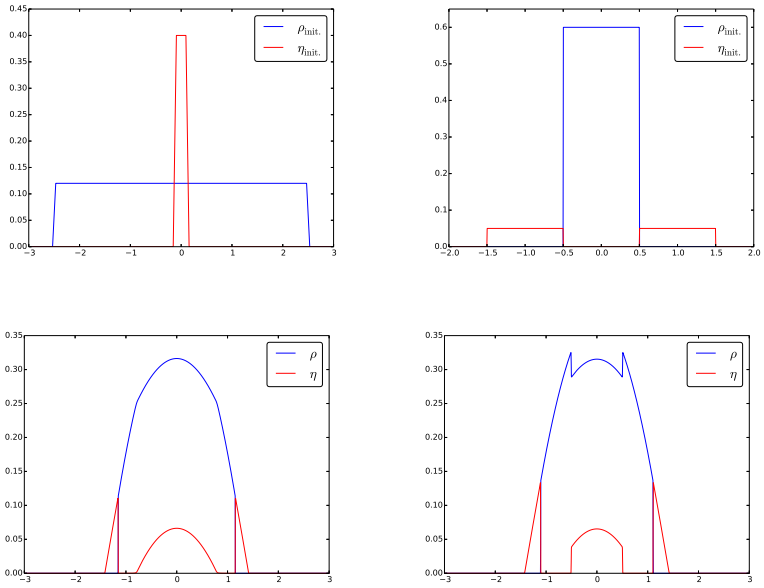

FIG. 6. *In all four graphs the masses are $m_1 = 0.1$, $m_2 = 0.6$, and the cross-diffusivity is $\epsilon = 1.7$. The first row depicts two different initial data—one (left) where η is included in ρ, and one (right) where η surrounds ρ. In the second row we present the corresponding steady states. Albeit having a similar make-up, they differ in their respective mass fraction of the corner, p. The left graph gives the minimal mass fraction $p_{\min}$, while the right graph gives the maximal, $p_{\max}$, respectively; cf. Figure 5.*

Let us impose nonnegativity of η at $x = b$, i.e., $\eta(b) \geq 0$. This is a reasonable assumption which is also reflected in the numerical simulations; cf. Figure 7(a). The figure shows steady states corresponding to the left initial data in Figure 6 as ϵ increases. While we observe a discontinuity of η at $x = b$ for small ϵ, there is a critical value where $\eta(b) = 0$ for all $\epsilon > \epsilon^{(1)}$. For the upper envelope we impose that the velocity field u_2 is nonnegative at $x = c$ since otherwise any small perturbation will render the stationary state unstable, i.e., mass would get transported into the interior; cf. Figure 7(b). These two conditions describe both envelopes in Figure 5.

Vanishing diffusion regime. In this section we study the case of Batman profiles as $\epsilon \to 0$. Recall the two equations for b and c,

$$(c-b)^2(3m_2 + 2cm_1 + m_1 b) + 3\epsilon(m_2 - m_1 + m_1 b - m_2 b) = 0, \tag{20}$$

$$m_1(c^2 - b^2) + \epsilon(m_1 + m_2) + 2m_2(c-b) - 2\sqrt{\epsilon}(m_2 + m_1 b)\cot\frac{b}{\sqrt{\epsilon}} = 0. \tag{21}$$

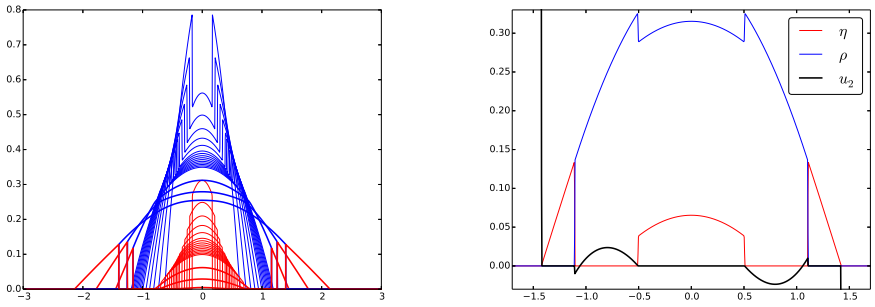

(a) $\eta(b) = 0$. (b) $u_2(c) > 0$.

FIG. 7. *Conditions for lower and upper boundary of the bifurcation diagram.*

When ϵ is small, both b and c are $O(\sqrt{\epsilon})$, suggesting

$$b = \epsilon^{1/2}\left(b_0 + \epsilon^{1/2} b_1 + \epsilon b_2 + \cdots\right) \quad \text{and} \quad c = \epsilon^{1/2}\left(c_0 + \epsilon^{1/2} c_1 + \epsilon c_2 + \cdots\right).$$

Upon substitution of the asymptotic expansions into (20) and (21), the leading order coefficients b_0 and c_0 satisfy

$$m_2 - m_1 + (c_0 - b_0)^2 m_2 = 0 \quad \text{and} \quad b_0 - c_0 + \cot b_0 = 0,$$

whence

$$b_0 = \operatorname{arccot}\sqrt{\frac{m_1 - m_2}{m_2}} \quad \text{and} \quad c_0 = \sqrt{\frac{m_1 - m_2}{m_2}} + \operatorname{arccot}\sqrt{\frac{m_1 - m_2}{m_2}}.$$

Notice that both densities in the Batman profiles will converge to a Dirac Delta at zero with the respective masses while keeping their shape with this described asymptotic scaling for their supports.

Asymmetric profiles. So far we only discussed symmetric steady states. However, there is an equally rich variety of nonsymmetric stationary states; cf. Figures 8 and 9. In Figure 8 we display the cases where the support only consists of three pieces—two regions inhabited by only one species and the middle one where both species coexist. Figure 9, on the other hand, shows three further examples of asymmetric steady states suggesting the existence of an infinite family of solution of asymmetric steady states. All states have the same qualitative profile in common but differ in their respective supports and mass distribution. We do not observe asymmetric profiles for $0 < \epsilon < \epsilon^{(1)}$ independent of the masses m_1 and m_2. Only for larger cross-diffusivities, $\epsilon > \epsilon^{(1)}$, can asymmetric profiles be observed. Moreover, there is a whole family of asymmetric profiles as can be seen in Figure 9. This is similar to the case of symmetric stationary states, parameterized by the mass fraction p.

Numerical stability of steady states and symmetrizing effect. Let us now discuss the numerical stability of the symmetric steady states. Here the bifurcation point $\epsilon^{(1)}$ plays an important role, for the system exhibits a symmetrizing effect whenever the cross-diffusivity lies below the critical one, in the sense that there is only one symmetric steady state attracting any initial data.

We fixed $\epsilon \in (0, \epsilon^{(1)})$ and chose $\rho_0 = 2m_1 \mathbb{1}_{[-0.5,0]}$ and $\eta_0 = 2m_2 \mathbb{1}_{[0,0.5]}$ for all combinations of masses of the form $(m_1, m_2) = 0.1 \cdot (i, j)$ for $i, j = 1, \ldots, 10$. In

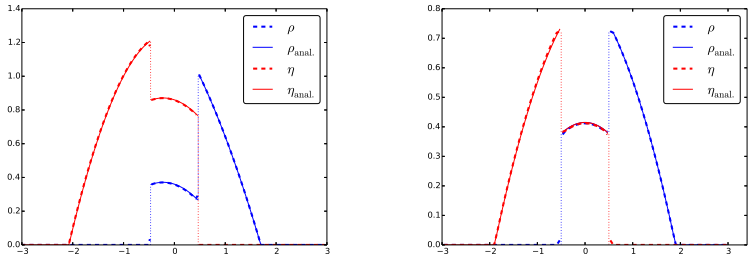

(a) Asymmetric profile for $m_1 = 1$, $m_2 = 2$, and $\epsilon = 3$.

(b) Antisymmetric profile for $m_1 = m_2 = 1$ and $\epsilon = 3$.

FIG. 8. *Nonsymmetric profiles for different masses (left) and equal masses (right), respectively.*

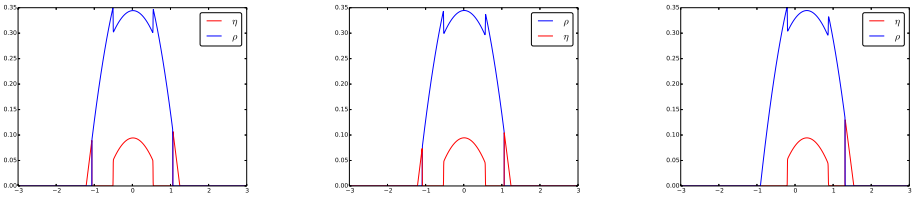

FIG. 9. *There is an infinite family of asymmetric steady states depending only on the initial data. Here* $m_1 = 0.6$, $m_2 = 0.1$, *and* $\epsilon = 1.2$. *The mass in the left corner decreases from left to right.*

all cases we observe that there is only one attractor, namely the Batman profile of the form given in Figures 2(b) and 3(b) in the case $m_1 = m_2$, respectively. For $\epsilon > \epsilon^{(1)}$ the system is not symmetrizing anymore and small perturbations lead to different stationary states. This can be seen if p is varied in $[p_{\min}, p_{\max}]$, for it leads to different states. A similar argument holds for the asymmetric states, by shifting mass from one corner into the other; cf. Figure 9.

4.2. Attractive-repulsive case. In this section we present the attractive-repulsive case, i.e., $W_{12} = |x| = -W_{21}$. Then the steady states have segregated densities, as asserted by the following proposition.

PROPOSITION 4.1 (completely segregated steady states). *Let* (ρ, η) *be a stationary solution of system* (2). *Then both species do not intermingle, i.e., there cannot be connected components of* $\operatorname{supp}(\rho) \cap \operatorname{supp}(\eta)$ *with nonempty interior.*

Proof. Suppose the interior of a connected component of $\operatorname{supp}(\rho) \cap \operatorname{supp}(\eta)$ is not empty. We know that both species satisfy (3) in that connected component:

$$c_1 = W_{11} \star \rho + W_{12} \star \eta + \epsilon(\rho + \eta),$$
$$c_2 = W_{22} \star \eta + W_{21} \star \rho + \epsilon(\rho + \eta).$$

Similar arguments as above imply that the interaction terms are twice differentiable in this interval; thus we differentiate twice and get

$$0 = m_1 + 2\eta + \epsilon(\rho + \eta)'' \quad \text{and} \quad 0 = m_2 - 2\rho + \epsilon(\rho + \eta)''. \tag{22}$$

Upon subtracting both equations we deduce $0 = m_1 - m_2 + 2(\rho+\eta)$ or, equivalently, $\rho + \eta = \frac{m_2 - m_1}{2}$. But then (22) reduces to $\eta = -m_1$ and $\rho = m_2$. Clearly this is a contradiction to the nonnegativity of the densities: $0 \le \eta = -m_1 < 0$. Thus the species do not intermingle. ∎

4.2.1. Steady states. This section is dedicated to studying the steady states of the system with attractive-repulsive cross-interactions. Due to numerical simulations and the previous proposition we make the following assumption on the support:

$$\operatorname{supp}(\rho) = [-c, c] \qquad \text{and} \qquad \operatorname{supp}(\eta) = [a, b] \cup [d, e],$$

where $a < b \le -c < c \le d < e$ are some real numbers. Using (3) we proceed similarly as above (cf. (8), (9)) to obtain

$$\eta^L(x) = \frac{1}{\epsilon}\left(c_2 - \frac{1}{2}m_2 x^2 + M_2 x - \frac{1}{2}\bar{M}_2 + M_1 - m_1 x\right),$$

for the shape of the second species on the left part of the support, and

$$\eta^R(x) = \frac{1}{\epsilon}\left(c_2 - \frac{1}{2}m_2 x^2 + M_2 x - \frac{1}{2}\bar{M}_2 - M_1 + m_1 x\right),$$

for the right part, respectively. Similarly as above, we can see that the interaction terms are twice differentiable. Therefore, differentiating (3) in the support of ρ twice yields $0 = m_1 + \epsilon(\rho)''$, and thus

$$\rho(x) = -\frac{1}{2\epsilon}m_1 x^2 + \beta x + \gamma,$$

with β, γ to be determined. Again we impose the continuity of the sum at the boundary points of each part of the supports, i.e.,

$$\eta^L(a) = 0, \quad \eta^L(b) = \rho(-c), \quad \rho(c) = \eta^R(d), \quad \text{and} \quad \eta^R(e) = 0, \tag{23}$$

where $\rho(-c) = 0$ if $b < -c$, and $\rho(c) = 0$ if $c < d$. We compute

$$\eta^L(x) = \eta^L(x) - \eta^L(a) = -\frac{1}{2\epsilon}m_2(x^2 - a^2) + \frac{M_2 - m_1}{\epsilon}(x - a),$$

and analogously

$$\eta^R(x) = \eta^R(x) - \eta^R(e) = -\frac{1}{2\epsilon}m_2(x^2 - e^2) + \frac{M_2 + m_1}{\epsilon}(x - e).$$

Concerning the first species, the parameters β, γ are determined by the continuity condition (23), and we obtain

$$\rho(x) = -\frac{1}{2\epsilon}m_1(x^2 - c^2) + \frac{\eta^R(d) - \eta^L(b)}{2c}x + \frac{\eta^R(d) + \eta^L(b)}{2}.$$

We can see that there are six unknowns, namely $a, b, c, d, e,$ and M_2 with a total of five conditions:

$$\int \rho \mathrm{d}x = m_1, \quad \int \eta^L \mathrm{d}x = \frac{1}{2}m_2, \quad \int \eta^R \mathrm{d}x = \frac{1}{2}m_2,$$
$$\int x\rho \mathrm{d}x = M_1, \quad \int x\eta \mathrm{d}x = M_2,$$

by imposing half of the mass of η to each side of ρ.

4.2.2. Case of strict segregation. Let us start by discussing the case

$$\eta^L(b) = \rho(\pm c) = \eta^R(d) = 0.$$

Then the condition on the mass yields

$$\int_{-c}^{c} \rho(x)\mathrm{d}x = m_1 \qquad \Rightarrow \qquad c = \sqrt[3]{\frac{3}{2}\epsilon}.$$

We can solve $\eta^L(b) = 0$ for a,

$$a = \frac{-m_2\, b + 2\, M_2 - 2\, m_1}{m_2}. \tag{24a}$$

Since half of the mass is located to the left of the first species, we get

$$\int_a^b \eta^L(x)\mathrm{d}x = \frac{m_2}{2} \quad \Rightarrow \quad b = \frac{\frac{1}{2}\sqrt[3]{6\epsilon}m_2 + M_2 - m_1}{m_2}, \tag{24b}$$

where we used (24a). Similarly, we solve $\eta^R(d) = 0$ for e to obtain

$$e = \frac{-m_2\, d + 2\, M_2 + 2\, m_1}{m_2}. \tag{24c}$$

Using this expression we compute

$$\int_d^e \eta^R(x)\,\mathrm{d}x = \frac{m_2}{2} \quad \Rightarrow \quad d = \frac{-\frac{1}{2}\sqrt[3]{6\,\epsilon}m_2 + M_2 + m_1}{m_2}. \tag{24d}$$

So we have determined c, b, d depending only on the masses and the second order moments of the second species, M_2. We can substitute the values into (24a), (24c) to determine a and e.

Critical ϵ and maximal M_2. We are interested in a condition determining as to when segregation of species occurs. In fact there is a critical value of the cross-diffusivity, ϵ_c, such that there only exist adjacent steady states for $\epsilon > \epsilon_c$. For $0 < \epsilon < \epsilon_c$ strictly segregated steady states occur if $|M_2| < M_{2,\max}$, where $M_2 = 0$ corresponds to the symmetric case. Figure 10 displays this behavior.

Let us derive an expression for ϵ_c and $M_{2,\max}$. For a fixed ϵ we may compute $M_{2,\max}$. We begin with the case $c = -b$. We can solve for the critical M_2, i.e.,

$$M_{2,\max} = -\frac{1}{2}m_2\sqrt[3]{\epsilon}(\sqrt[3]{12} + \sqrt[3]{6}) + m_1. \tag{25}$$

Similarly, we can solve equation $c = d$ for M_2, which gives

$$\bar{M_2} = \frac{1}{2}m_2\sqrt[3]{\epsilon}(\sqrt[3]{12} + \sqrt[3]{6}) - m_1 = -M_{2,\max}. \tag{26}$$

Thus, the parameter M_2 can vary in the range $[-M_{2,\max}, M_{2,\max}]$. Then the critical value of ϵ makes this interval degenerate, i.e., it is given by the condition $M_{2,\max} = 0$. This way we obtain

$$\epsilon_c = \frac{4}{9}\,\frac{m_1^3\left(\sqrt[3]{2} - 1\right)}{m_2^3}.$$

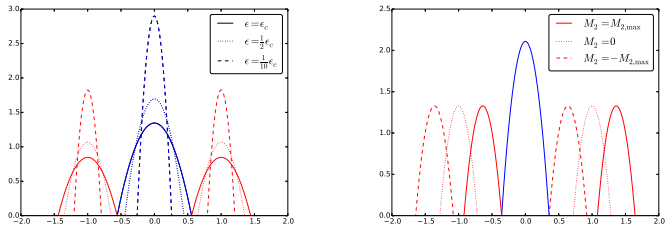

(a) Critical ϵ. (b) Maximal M_2.

FIG. 10. *Left: If $\epsilon \in (0, \epsilon_c)$, strictly segregated distributions are possible (dashed/dotted). If $\epsilon = \epsilon_c$, both species touch (straight line), and for $\epsilon > \epsilon_c$ strictly segregated states are no longer possible. Right: In the case $\epsilon \in (0, \epsilon_c)$ there exists a whole spectrum of steady states, parameterized by M_2 ranging from $-M_{2,\max}$ (dashed) to $M_{2,\max}$ (straight line). The case $M_2 = 0$ corresponds to the symmetric case.*

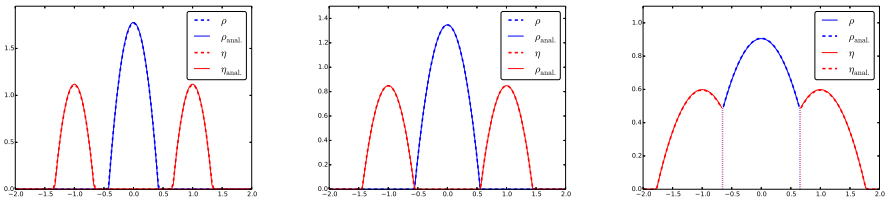

(a) $\epsilon = 1/20$. (b) $\epsilon = \frac{4}{9}(2^{1/3} - 1)$. (c) $\epsilon = 1/2$.

FIG. 11. *Stationary distributions for same initial data and mass. For $\epsilon < \epsilon_c$ both species are strictly segregated. For $\epsilon > \epsilon_c$ both species are adjacent and they touch at $x = \pm c$ for the critical value of ϵ.*

If $\epsilon = \epsilon_c$, both species touch at the points $\{-c, c\}$ or are partially adjacent. If $\epsilon < \epsilon_c$, but we choose M_2 outside of the aforementioned range, we observe steady states consisting of (partially) adjacent bumps.

Figure 11 displays the steady states in the symmetric case, i.e., $M_2 = 0$, for attractive-repulsive cross-interactions. We observe a transition of behavior for different values of ϵ, ranging from strictly segregated states to completely adjacent states. The numerical results agree perfectly with the results obtained analytically.

Vanishing diffusion regime. As we have seen in Figure 10, there is an ϵ_c such that the steady states parameterized by $M_2 \in [-M_{2,\max}, M_{2,\max}]$ are segregated. In this section we consider the case of vanishing cross-diffusion. We can assume that $\epsilon < \epsilon_c$ and $M_2 \in [M_{2,\min}, M_{2,\max}]$. Then (24) determines the support of all densities. We can rewrite the support as follows:

$$\begin{aligned}
\operatorname{supp}(\eta^L) &= \frac{M_2 - m_1}{m_2} - (3/4\epsilon)^{1/3}\,[-1, 1], \\
\operatorname{supp}(\rho) &= (3/4\epsilon)^{1/3}\,[-1, 1], \\
\operatorname{supp}(\eta^R) &= \frac{M_2 + m_1}{m_2} + (3/4\epsilon)^{1/3}\,[-1, 1].
\end{aligned}$$

We see that the support shrinks to the single points

$$\operatorname{supp}(\eta^L) = \left\{ \frac{M_2 - m_1}{m_2} \right\}, \quad \operatorname{supp}(\rho) = \{0\}, \quad \text{and} \quad \operatorname{supp}(\eta^R) = \left\{ \frac{M_2 + m_1}{m_2} \right\},$$

and $M_2 \in (-m_1, m_1)$ with steady states

$$\rho = \delta_0 \qquad \text{and} \qquad \eta = \frac{1}{2}\left(\delta_{\frac{M_2 - m_1}{m_2}} + \delta_{\frac{M_2 + m_1}{m_2}} \right). \tag{27}$$

This is indeed a measure solution of the system. To see this let us consider

$$\begin{aligned}
\dot{X} &= -\frac{m_2}{2} W_{12}'(X - Y_1) - \frac{m_2}{2} W_{12}'(X - Y_2), \\
\dot{Y}_1 &= -\frac{m_2}{2} W_{22}'(Y_1 - Y_2) - m_1 W_{21}'(Y_1 - X), \\
\dot{Y}_2 &= -\frac{m_2}{2} W_{22}'(Y_2 - Y_1) - m_1 W_{21}'(Y_2 - X).
\end{aligned}$$

Since we are looking for a steady state we observe

$$\dot{X} = 0 \quad \Leftrightarrow \quad \begin{cases} X - Y_1 > 0 \wedge X - Y_2 < 0 & \text{or} \\ X - Y_1 < 0 \wedge X - Y_2 > 0. \end{cases}$$

We assume without loss of generality that $X - Y_1 > 0 \wedge X - Y_2 < 0$, i.e., $Y_1 < X < Y_2$. From $\dot{Y}_1 = 0$ a short computation yields

$$Y_2 - Y_1 = 2\frac{m_1}{m_2}.$$

Fixing $X = 0$ we get $Y_2 = Y_1 + 2m_1/m_2$ and $Y_1 \in [-2\frac{m_1}{m_2}, 0]$. This is exactly the solution of the system as $\epsilon \to 0$; cf. (27).

Numerical stability of steady states. Here we want to discuss the stability of the stationary states of the attractive-repulsive system. In general, the stationary states are not stable as small perturbations may lead to a completely different stationary state. It becomes clear in Figure 10 that perturbing η by shifting it to either side leads to a completely different stationary state. Although this is an arbitrarily small perturbation in any L^p-norm, the translated profile is another stationary state. This is why these profiles are not stable. The same argument holds for symmetric stationary states. However, they are stable under symmetric perturbations since any symmetric initial data is attracted by the symmetric profile. Characterizing fully the basin of attraction for each stationary state seems difficult. For perturbations shifting mass from η^L to η^R (or vice versa) there is no stationary state, but the profile is then attracted by a travelling pulse solution.

4.2.3. Travelling pulses. In addition to the convergence to steady states we observe travelling pulse solutions in the case of attractive-repulsive cross-interactions. We observe two types of travelling pulses—those consisting of two bumps and those consisting of three.

In our numerical study we do not observe more than three bumps, even in the case of exponentially decaying potentials. There are, however, metastable states where more bumps exist, but after a sufficiently long time they collapse into two or three.

Two pulses. In order to compute these profiles, we assume $[-a, a]$ denotes the initial support of $u = \eta(0)$ and, therefore, $[-a - x_0, a - x_0]$ the initial support of $\rho(0)$. Let us denote by m and M the mass of u and its first moment, respectively.

We transform the system into comoving coordinates, $z = x - vt$, and obtain the following conditions for the pulse profiles:

$$\begin{aligned} c_1 &= (W_{11} \star u)(z + x_0) + (W_{12} \star u)(z) + \epsilon u(z + x_0) + vz \quad \text{on } [-a - x_0, a - x_0], \\ c_2 &= (W_{22} \star u)(z) + (W_{21} \star u)(z + x_0) + \epsilon u(z) + vz \quad \text{on } [-a, a], \end{aligned}$$

similarly to (3). A computation similar to (8), (9) leads to the explicit form of the pulse,

$$u(z) = -\frac{1}{2\epsilon} m z^2 + \frac{M + m - v}{\epsilon} z + \tilde{c}_1,$$

on $[-a, a]$ for some constant $\tilde{c}_1$. Since $u(z)$ is a parabola with roots $\pm a$, u is symmetric. As a consequence we obtain $M = v - m$. By definition of $M = \int z u(z) \mathrm{d}z = 0$, and thus $v = m$. Hence the shape is given by

$$u(z) = u(z) - u(a) = -\frac{1}{2\epsilon} m (z^2 - a^2). \tag{28}$$

Then the following consideration determines the boundary of the support, a:

$$\int_{-a}^{a} u(z) \mathrm{d}z = m \quad \Rightarrow \quad a = \sqrt[3]{\frac{3\epsilon}{2}}. \tag{29}$$

Finally, the distance between both profiles, x_0, is arbitrary so long as it does not lead to an overlap of both pulses, i.e., $x_0 \geq 2a$, because both profiles are moving at the same speed.

Lastly, let us show that there are no adjacent solutions that are solutions whose support is of the form

$$\mathrm{supp}(u_1) = [-a, 0] \qquad \text{and} \qquad \mathrm{supp}(u_2) = [0, a].$$

If there were travelling pulse solutions of this form, they would satisfy the same equations as above. Then,

$$\begin{aligned} u_1(z) &= -\frac{1}{2\epsilon} m (z^2 - a^2) + \frac{M + m - v}{\epsilon} (z + a) \quad \text{on } [-a, 0], \\ u_2(z) &= -\frac{1}{2\epsilon} m (z^2 - a^2) + \frac{M + m - v}{\epsilon} (z - a) \quad \text{on } [0, a]. \end{aligned}$$

The continuity of the sum suggests that $u_1(0) = u_2(0)$ implies $m = v$. But then

$$\int_0^a z u_2(z) \mathrm{d}z = M \qquad \Rightarrow \qquad M = \frac{3}{4} \frac{m a^4}{5\, a^3 - 6\, \epsilon}.$$

We solve this expression for $a > 0$ and find $a = \sqrt[3]{12\epsilon}$. A comparison of the support of the adjacent solutions and the support of segregated solutions (cf. (29)) shows that the adjacent solutions in fact only touch.

Figure 12 shows the formation of two travelling pulses. We start with two indicator functions as initial data and let the system evolve. At about time $t \approx 2$ we observe

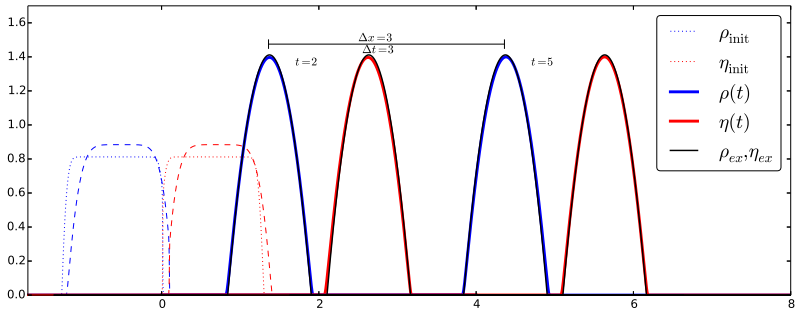

FIG. 12. *The initial data is given by the dotted graph, and the dashed lines are an intermediate solution. After some time $t \approx 2$ the travelling pulse profile is established. The pulses move at velocity $v = m = 1$ as can be seen in the graph, since $\Delta x = \Delta t = 3$.*

a fully established pulse profile. We let the system evolve further and compare the solution at $t = 5$ with the solution at time $t = 2$. The figure shows that the shapes do not change any further but are only transported at a velocity of $v = \Delta x/\Delta t = 1$ in perfect agreement with the analytical result, $v = m$.

Subsequently, we shall see that the solution consisting of two pulses is in fact a special case of the three-pulses configurations. The latter consist of the first species, ρ, surrounded by the second species, η. We assume

$$\text{supp}(\rho) = [-c, c] \qquad \text{and} \qquad \text{supp}(\eta) = [a, b] \cup [d, e],$$

where $a < b \le -c < c \le d < e$ are real numbers and

$$\rho(t, x) = \rho(x - vt) \qquad \text{and} \qquad \eta(t, x) = \eta(x - vt).$$

We transform to comoving coordinates, $z = x - vt$, and obtain the following conditions for the profile:

$$\begin{aligned} c_1 &= (W_{11} \star \rho)(z) + (W_{12} \star \eta)(z) + \epsilon\rho(z) + vz \quad \text{on } [-c, c], \\ c_2 &= (W_{22} \star \eta)(z) + (W_{21} \star \rho)(z) + \epsilon\eta(z) + vz \quad \text{on } [a, b] \cup [d, e], \end{aligned}$$

whence we obtain

$$\rho(z) = -\frac{1}{2\epsilon} m z^2 + \frac{(m^R - m^L) - v}{\epsilon} z + \tilde{c}_1. \tag{30}$$

Here

$$m^L = \int_a^b \eta(z)\mathrm{d}z \qquad \text{and} \qquad m^R = \int_d^e \eta(z)\mathrm{d}z. \tag{31}$$

Similarly, the profiles of the second species are given by

$$\eta^L(z) = -\frac{1}{2\epsilon} m(z^2 - a^2) + \frac{M_2 - m - v}{\epsilon}(z - a) \qquad \text{on } [a, b]$$

and

$$\eta^R(z) = -\frac{1}{2\epsilon} m(z^2 - e^2) + \frac{M_2 + m - v}{\epsilon}(z - e) \qquad \text{on } [d, e].$$

Again, we use the fact that the sum of both densities has to be continuous, i.e.,

$$\eta^L(a) = 0, \quad \eta^L(b) = \rho(-c), \quad \rho(c) = \eta^R(d), \quad \text{and} \quad \eta^R(e) = 0,$$

where $\rho(-c) = 0$ if $b < -c$, and $\rho(c) = 0$ if $c < d$. In addition, the conditions on the masses

$$m = \int_{-c}^{c} \rho(z)\mathrm{d}z, \tag{32}$$

as well as (31) hold. We consider the case of strictly segregated solutions first, i.e., $b < -c$ and $c < d$. Since then $\rho(\pm c) = 0$, we may deduce from (30) that $v = m^R - m^L$ for the speed of propagation and

$$\rho(z) = -\frac{1}{2\epsilon} m(z^2 - c^2), \qquad \text{with } c = \sqrt[3]{\frac{3}{2}\epsilon},$$

for the shape of the first species (c is determined by the mass condition, (32)). Furthermore we obtain

$$\eta^L(b) = 0 \quad \Rightarrow \quad a = \frac{-mb + 2M_2 - 2m - 2v}{m}, \tag{33a}$$

in terms of b. Similarly, we can get an expression for e in terms of d, i.e.,

$$\eta^R(d) = 0 \quad \Rightarrow \quad e = \frac{-md + 2M_2 + 2m - 2v}{m}. \tag{33b}$$

Using the expression for a, we obtain

$$\int_a^b \eta^L(x)\mathrm{d}x = m^L \quad \Rightarrow \quad b = \frac{\sqrt[3]{\frac{3}{2}\epsilon m^2 m^L} + M_2 - m - v}{m}. \tag{33c}$$

Now we employ the expression for e to get

$$\int_d^e \eta^R(x)\mathrm{d}x = m^R \quad \Rightarrow \quad d = \frac{-\sqrt[3]{\frac{3}{2}\epsilon m^2 m^R} + M_2 + m - v}{m}. \tag{33d}$$

Note that the collection of equations (33) completely determine the support and the profiles of the pulses. Figure 13 shows the formation of a triple pulse solution. We choose characteristic functions as initial data (dotted). The mass on the left is $m^L = 1/3$ and, respectively, $m^R = 2/3$ on the right. After some time the pulse profile is established. We compare the system (blue and red) at time $t = 9$ and time $t = 24$ with the analytical expression derived above (black). The figure displays a great agreement between our numerical result and the analytical. Once the profile is fully established it moves to the right at a constant speed. The numerical velocity is given by $\Delta x/\Delta t = 5/15 = 1/3$. This is in perfect agreement with the analytically obtained results, i.e., $v = m^R - m^L = 2/3 - 1/3 = 1/3$.

At this stage, let us draw our attention to two special cases.

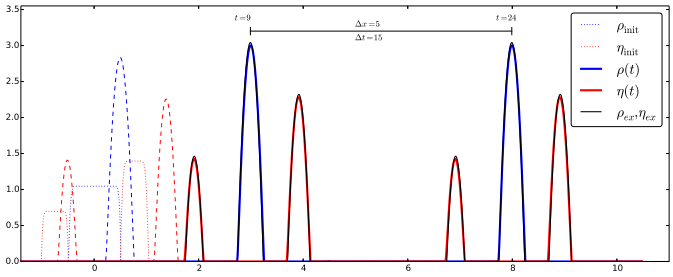

FIG. 13. *Travelling pulse solution consisting of three pulses. The mass of the second species amounts to* $m^L = 1/3$ *on the left and to* $m^R = 2/3$ *on the right, respectively. The dotted lines represent the initial data and the dashed lines represent an intermediate solution. After some time,* $t \approx 9$*, the pulse profiles have been established and both species move to the right at a velocity of* $v = \Delta x/\Delta t = 1/3$*. The thick red and blue lines correspond to the numerical solution, the black lines to the analytically computed travelling pulse solution. (Figure appears in color online.)*

Remark 1. First, we consider the case $m^L = 0$. In this case $v = m^R - m^L = m$. Thus, in conjunction with (33a), (33c) there holds $b = \frac{M_2}{m} = a$, i.e., the left part is degenerate. Moreover, the support of the right part is

$$d = -\sqrt[3]{\frac{3}{2}\epsilon} + \frac{M_2}{m},$$

according to (33d). We substitute this into (33b) and get

$$e = \frac{-md + 2M_2}{m} = \sqrt[3]{\frac{3}{2}\epsilon} + \frac{M_2}{m}.$$

Thus we can write the support in the following form: $\big[-\sqrt[3]{\frac{3}{2}\epsilon}, \sqrt[3]{\frac{3}{2}\epsilon}\big] + \frac{M_2}{m}$. Let us have a closer look at η^R now. Using $e = c + \frac{M_2}{m}$ we obtain

$$\eta^R(z) = -\frac{1}{2\epsilon} m \left(z - \frac{M_2}{m} - c\right)\left(z - \frac{M_2}{m} + c\right),$$

where we set $x_0 := M_2/m$. Thus we finally obtain

$$\eta^R(z) = -\frac{1}{2\epsilon} m((z - x_0)^2 - c^2),$$

supported on the interval $[-c + x_0, c + x_0]$. This is precisely the solution to the two-pulse system; cf. (28).

Remark 2. The second remark concerns the case $m^R = m^L$. Then $v = 0$ and, according to (33c), (33d), we get

$$b = \left(\sqrt[3]{\frac{3}{4}\epsilon} - 1\right) + \frac{M_2}{m} \quad \text{and} \quad d = -\left(\sqrt[3]{\frac{3}{4}\epsilon} - 1\right) + \frac{M_2}{m},$$

which are equal to (24b), (24d) in the case $m = m_1 = m_2$. In addition, (33a), (33b) turn into (24a), (24c), i.e., the support of the triple pulse solutions agrees with the support of the fully segregated steady states. Similarly, the shapes agree in the case $v = 0$.

Remark 3 (maximal M_2). Let us get back to the general case. We study the interval of M_2. Assuming ϵ fixed, $b = -c$ yields

$$M_{2,\max} = \frac{1}{2}\sqrt[3]{12\epsilon}m + \frac{1}{2}\sqrt[3]{12m_R\,\epsilon\,m^2} - m_1 + v.$$

On the other hand, $c = d$ gives

$$M_{2,\min} = -\frac{1}{2}\sqrt[3]{12\epsilon}m - \frac{1}{2}\sqrt[3]{12m_L\,\epsilon\,m^2} + m + v,$$

where $v = m^R - m^L$, as above. It is worthwhile noting that in the case $m^L = m^R$ both $M_{2,\max}$ and $M_{2,\min}$ coincide with (25), (26) for the stationary state.

Parallel to the consideration for (partially) adjacent steady states of the attractive-repulsive system we also find the existence of adjacent travelling pulse solutions.

5. Generality. This section is dedicated to the study of more general or realistic potentials to understand whether the behaviors observed above are specific to our interaction potentials. Different cross-interaction and self-interaction potentials will be investigated. Even though analytic expressions for the steady states and travelling pulses seem no longer available, the behaviors are indeed generic and, in fact, even richer than the above particular model.

5.1. Different cross-interactions. Let us begin by considering different cross-interaction potentials. We regard two types of potentials—power laws and Morse-like potentials decaying at infinity, i.e.,

$$W_{12} = |x|^p = \pm W_{21} \quad \text{and} \quad W_{12} = 1 - \exp(-|x|^p) = \pm W_{21},$$

where $p \in \{1/2, 1, 3/2\}$. This choice of potentials is motivated as they are similar to the Newtonian cross-interaction.

In both cases, we observe a very similar behavior in both the mutually attractive case and the attractive-repulsive case, respectively. Figure 14 displays the Batman profile for different cross-interaction potentials. In all simulations the same initial data, mass, and cross-diffusivity were used. Each steady state features the salient characteristics observed in the case $W_{cr} = |x|$, i.e., a region of coexistence surrounded by regions inhabited by only one species. From the steady states we can also infer other information, namely, second type profiles exist and the point of bifurcation depends on the potential, for only Figure 14(d) exhibits a profile of second type. Similarly, we observe a symmetrizing effect for small cross-diffusivities and asymmetric profiles.

5.2. Different self-interactions. Here, we keep the cross-interaction potentials fixed as $W_{12} = |x| = \pm W_{21}$ and consider different self-interaction potentials of the form $W(x) = |x|^p/p$, for $p \in \{3/2, 2, 4\}$. In each case we observe a very similar behavior. We obtain the same variety including both Batman profiles and the profiles of second type. Again we observe that the system is symmetrizing; however, it is for a different $\epsilon^{(1)}$. In the attractive-repulsive case as well we observe the characteristic profiles and the formation of pulses.

6. Conclusions. In this paper we introduced a system of two interacting species with cross-diffusion as the natural extension of the aggregation equation from one single species. We proposed a positivity preserving finite volume scheme and used it in order to study the system numerically. For a specific choice of potentials, the steady states could be constructed with parameters governed by algebraic equations. The

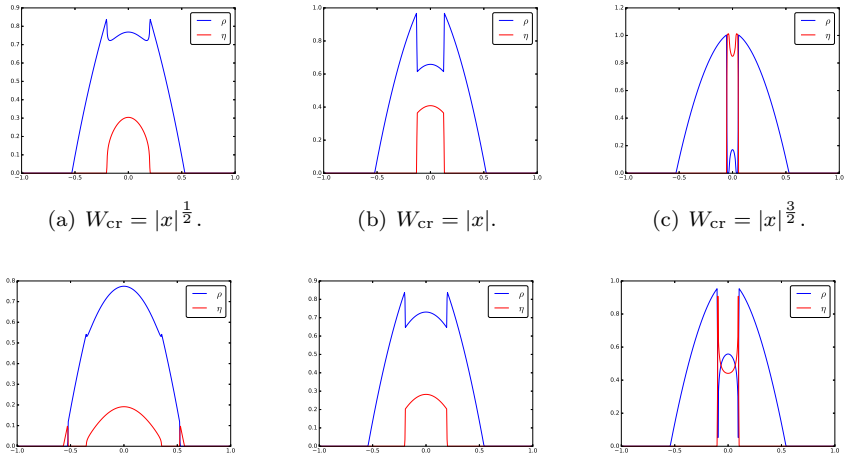

(a) $W_{\rm cr} = |x|^{\frac{1}{2}}$. (b) $W_{\rm cr} = |x|$. (c) $W_{\rm cr} = |x|^{\frac{3}{2}}$.

(d) $W_{\rm cr} = 1 - \exp(-|x|^{\frac{1}{2}})$. (e) $W_{\rm cr} = 1 - \exp(-|x|)$. (f) $W_{\rm cr} = 1 - \exp(-|x|^{\frac{3}{2}})$.

FIG. 14. *The Batman profiles for different interaction potentials.*

availability of analytical expressions of the stationary states is of great importance as they can be used to test the effectiveness of related numerical schemes. In our study we found that these analytically constructed stationary states agree extremely well with those simulated with our proposed scheme, and similar agreements were observed for travelling pulses as well. We observed that the finite volume scheme copes very well with the occurrence of jump discontinuities which is of high significance as only the sum of the two densities appears to be continuous. Using the same scheme the model was explored for related potentials and the behaviors observed for the specific potentials turned out to be generic, when the cross-interaction potentials or the self-interaction potentials were exchanged. While this paper gives a first insight as to what qualitative properties can be expected from models taking the general form (1), there is still a lot of analytical work to be done. First and foremost, it is still an open problem to show the existence of solutions to the systems. The formal gradient flow structure is lost when the cross-interaction potentials W_{12} and W_{21} are not proportional to each other, and the main problem is to find the right estimates for individual species since we only control the gradient of the sum of the densities.

REFERENCES

[1] D. BALAGUÉ, J. A. CARRILLO, T. LAURENT, AND G. RAOUL, *Dimensionality of local minimizers of the interaction energy*, Arch. Ration. Mech. Anal., 209 (2013), pp. 1055–1088, https://doi.org/10.1007/s00205-013-0644-6.

[2] D. BENEDETTO, E. CAGLIOTI, AND M. PULVIRENTI, *A kinetic equation for granular media*, RAIRO Modél. Math. Anal. Numér., 31 (1997), pp. 615–641.

[3] A. L. BERTOZZI, J. A. CARRILLO, AND T. LAURENT, *Blow-up in multidimensional aggregation equations with mildly singular interaction kernels*, Nonlinearity, 22 (2009), pp. 683–710, https://doi.org/10.1088/0951-7715/22/3/009.

[4] A. L. BERTOZZI, T. KOLOKOLNIKOV, H. SUN, D. UMINSKY, AND J. VON BRECHT, *Ring patterns and their bifurcations in a nonlocal model of biological swarms*, Commun. Math. Sci., 13 (2015), pp. 955–985, https://doi.org/10.4310/CMS.2015.v13.n4.a6.

[5] M. BERTSCH, R. DAL PASSO, AND M. MIMURA, *A free boundary problem arising in a simplified tumour growth model of contact inhibition*, Interfaces Free Bound., 12 (2010), pp. 235–250.

[6] M. Bertsch, M. Gurtin, and D. Hilhorst, *On a degenerate diffusion equation of the form $c(z)_t = \varphi(z_x)_x$ with application to population dynamics*, J. Differential Equations, 67 (1987), pp. 56–89.

[7] M. Bertsch, M. Gurtin, and D. Hilhorst, *On interacting populations that disperse to avoid crowding: The case of equal dispersal velocities*, Nonlinear Anal., 11 (1987), pp. 493–499.

[8] M. Bodnar and J. J. L. Velázquez, *Friction dominated dynamics of interacting particles locally close to a crystallographic lattice*, Math. Methods Appl. Sci., 36 (2013), pp. 1206–1228, https://doi.org/10.1002/mma.2672.

[9] M. Burger, V. Capasso, and D. Morale, *On an aggregation model with long and short range interactions*, Nonlinear Anal. Real World Appl., 8 (2007), pp. 939–958, https://doi.org/10.1016/j.nonrwa.2006.04.002.

[10] M. Burger, M. Di Francesco, S. Fagioli, and A. Stevens, *Sorting Phenomena in a Mathematical Model for Two Mutually Attracting/Repelling Species*, preprint, https://arxiv.org/abs/1704.04179, 2017.

[11] M. Burger, R. Fetecau, and Y. Huang, *Stationary states and asymptotic behavior of aggregation models with nonlinear local repulsion*, SIAM J. Appl. Dyn. Syst., 13 (2014), pp. 397–424, https://doi.org/10.1137/130923786.

[12] V. Calvez and J. A. Carrillo, *Volume effects in the Keller-Segel model: Energy estimates preventing blow-up*, J. Math. Pures Appl. (9), 86 (2006), pp. 155–175, https://doi.org/10.1016/j.matpur.2006.04.002.

[13] V. Calvez, J. A. Carrillo, and F. Hoffmann, *Equilibria of Homogeneous Functionals in the Fair-competition Regime*, preprint, https://arxiv.org/abs/1610.00939, 2016.

[14] V. Calvez, J. A. Carrillo, and F. Hoffmann, *The Geometry of Diffusing and Self-attracting Particles in a One-dimensional Fair-competition Regime*, preprint, https://arxiv.org/abs/1612.08225, 2016.

[15] J. A. Carrillo, A. Chertock, and Y. Huang, *A finite-volume method for nonlinear nonlocal equations with a gradient flow structure*, Commun. Comput. Phys., 17 (2015), pp. 233–258.

[16] J. A. Carrillo, Y.-P. Choi, and M. Hauray, *The derivation of swarming models: Mean-field limit and Wasserstein distances*, in Collective Dynamics from Bacteria to Crowds, CISM Courses and Lect. 553, Springer, Vienna, 2014, pp. 1–46, https://doi.org/10.1007/978-3-7091-1785-9_1.

[17] J. A. Carrillo, M. G. Delgadino, and A. Mellet, *Regularity of local minimizers of the interaction energy via obstacle problems*, Comm. Math. Phys., 343 (2016), pp. 747–781, https://doi.org/10.1007/s00220-016-2598-7.

[18] J. A. Carrillo, M. DiFrancesco, A. Figalli, T. Laurent, and D. Slepčev, *Global-in-time weak measure solutions and finite-time aggregation for nonlocal interaction equations*, Duke Math. J., 156 (2011), pp. 229–271.

[19] J. A. Carrillo, M. R. D'Orsogna, and V. Panferov, *Double milling in self-propelled swarms from kinetic theory*, Kinet. Relat. Models, 2 (2009), pp. 363–378, https://doi.org/10.3934/krm.2009.2.363.

[20] J. A. Carrillo, M. Fornasier, G. Toscani, and F. Vecil, *Particle, kinetic, and hydrodynamic models of swarming*, in Mathematical Modeling of Collective Behavior in Socio-economic and Life Sciences, Birkhäuser Boston, Boston, 2010, pp. 297–336.

[21] J. A. Carrillo, Y. Huang, and S. Martin, *Explicit flock solutions for quasi-Morse potentials*, European J. Appl. Math., 25 (2014), pp. 553–578, https://doi.org/10.1017/S0956792514000126.

[22] J. A. Carrillo, S. Martin, and V. Panferov, *A new interaction potential for swarming models*, Phys. D, 260 (2013), pp. 112–126, https://doi.org/10.1016/j.physd.2013.02.004.

[23] F. Cucker and S. Smale, *Emergent behavior in flocks*, IEEE Trans. Automat. Control, 52 (2007), pp. 852–862.

[24] M. Di Francesco and S. Fagioli, *Measure solutions for non-local interaction PDEs with two species*, Nonlinearity, 26 (2013), pp. 2777–2808.

[25] P. Domschke, D. Trucu, A. Gerisch, and M. A. J. Chaplain, *Mathematical modelling of cancer invasion: Implications of cell adhesion variability for tumour infiltrative growth patterns*, J. Theoret. Biol., 361 (2014), pp. 41–60, https://doi.org/10.1016/j.jtbi.2014.07.010.

[26] M. R. D'Orsogna, Y.-L. Chuang, A. L. Bertozzi, and L. S. Chayes, *Self-propelled particles with soft-core interactions: Patterns, stability, and collapse*, Phys. Rev. Lett., 96 (2006), 104302.

[27] J. H. M. Evers and T. Kolokolnikov, *Metastable states for an aggregation model with noise*, SIAM J. Appl. Dyn. Syst., 15 (2016), pp. 2213–2226, https://doi.org/10.1137/16M1069006.

[28] R. C. Fetecau and Y. Huang, *Equilibria of biological aggregations with nonlocal repulsive-attractive interactions*, Phys. D, 260 (2013), pp. 49–64, https://doi.org/10.1016/j.physd.2012.11.004.

[29] R. C. Fetecau, Y. Huang, and T. Kolokolnikov, *Swarm dynamics and equilibria for a nonlocal aggregation model*, Nonlinearity, 24 (2011), pp. 2681–2716, https://doi.org/10.1088/0951-7715/24/10/002.

[30] A. Gerisch and M. A. J. Chaplain, *Mathematical modelling of cancer cell invasion of tissue: Local and non-local models and the effect of adhesion*, J. Theoret. Biol., 250 (2008), pp. 684–704, https://doi.org/10.1016/j.jtbi.2007.10.026.

[31] M. E. Gurtin and A. Pipkin, *A note on interacting populations that disperse to avoid crowding*, Quart. Appl. Math., 42 (1984), pp. 87–94.

[32] T. Hillen and K. Painter, *Global existence for a parabolic chemotaxis model with prevention of overcrowding*, Adv. in Appl. Math., 26 (2001), pp. 280–301.

[33] R. Jordan, D. Kinderlehrer, and F. Otto, *The variational formulation of the Fokker–Planck equation*, SIAM J. Math. Anal., 29 (1998), pp. 1–17, https://doi.org/10.1137/S0036141096303359.

[34] J. Jost and X. Li-Jost, *Calculus of Variations*, Cambridge Stud. Adv. Math. 64, Cambridge University Press, Cambridge, UK, 1998.

[35] T. Kolokolnikov, J. A. Carrillo, A. Bertozzi, R. Fetecau, and M. Lewis, *Emergent behaviour in multi-particle systems with non-local interactions*, Phys. D, 260 (2013), pp. 1–4, https://doi.org/10.1016/j.physd.2013.06.011.

[36] T. Kolokolnikov, H. Sun, D. Uminsky, and A. L. Bertozzi, *Stability of ring patterns arising from two-dimensional particle interactions*, Phys. Rev. E, 84 (2011), 015203, https://doi.org/10.1103/PhysRevE.84.015203.

[37] A. Mackey, T. Kolokolnikov, and A. L. Bertozzi, *Two-species particle aggregation and stability of co-dimension one solutions*, Discrete Contin. Dyn. Syst. Ser. B, 19 (2014), pp. 1411–1436.

[38] A. Mogilner and L. Edelstein-Keshet, *A non-local model for a swarm*, J. Math. Biol., 38 (1999), pp. 534–570.

[39] H. Murakawa and H. Togashi, *Continuous models for cell–cell adhesion*, J. Theoret. Biol., 374 (2015), pp. 1–12.

[40] K. Oelschläger, *Large systems of interacting particles and the porous medium equation*, J. Differential Equations, 88 (1990), pp. 294–346, https://doi.org/10.1016/0022-0396(90)90101-T.

[41] K. Painter and T. Hillen, *Volume-filling and quorum-sensing in models for chemosensitive movement*, Can. Appl. Math. Q., 10 (2002), pp. 501–543.

[42] K. J. Painter, J. M. Bloomfield, J. A. Sherratt, and A. Gerisch, *A nonlocal model for contact attraction and repulsion in heterogeneous cell populations*, Bull. Math. Biol., 77 (2015), pp. 1132–1165, https://doi.org/10.1007/s11538-015-0080-x.

[43] J. Saragosti, V. Calvez, N. Bournaveas, A. Buguin, P. Silberzan, and B. Perthame, *Mathematical description of bacterial traveling pulses*, PLoS Comput. Biol., 6 (2010), e1000890, https://doi.org/10.1371/journal.pcbi.1000890.

[44] N. Shigesada, *Spatial distribution of dispersing animals*, J. Math. Biol., 9 (1980), pp. 85–96.

[45] N. Shigesada, K. Kawasaki, and E. Teramoto, *Spatial segregation of interacting species*, J. Theoret. Biol., 79 (1979), pp. 83–99, https://doi.org/10.1016/0022-5193(79)90258-3.

[46] H. Togashi, K. Kominami, M. Waseda, H. Komura, J. Miyoshi, M. Takeichi, and Y. Takai, *Nectins establish a checkerboard-like cellular pattern in the auditory epithelium*, Science, 333 (2011), pp. 1144–1147.

[47] C. M. Topaz, A. L. Bertozzi, and M. A. Lewis, *A nonlocal continuum model for biological aggregation*, Bull. Math. Biol., 68 (2006), pp. 1601–1623, https://doi.org/10.1007/s11538-006-9088-6.

[48] G. Toscani, *One-dimensional kinetic models of granular flows*, M2AN Math. Model. Numer. Anal., 34 (2000), pp. 1277–1291.

[49] A. Volkening and B. Sandstede, *Modelling stripe formation in zebrafish: An agent-based approach*, Journal of The Royal Society Interface, 12 (2015), https://doi.org/10.1098/rsif.2015.0812.